Elsevier Editorial System(tm) for
Construction & Building Materials
Manuscript Draft

Manuscript Number: CONBUILDMAT-D-19-07940R1

Title: Hydration mechanisms of Ba-doped ye'elimite: Effect of Ba/Ca ratio on hydration behavior

Article Type: Research Paper

Keywords: ye'elimite; hydration mechanism; Rietveld; C4-xBxA3$

Corresponding Author: Professor Piqi Zhao,

Corresponding Author's Institution:

First Author: Piqi Zhao

Order of Authors: Piqi Zhao; Xingyuan Bao; Heng Chen; Shoude Wang; Lingchao Lu; Angeles. G De la Torre; Xin Cheng

Abstract: Ba-doped ye'elimite, abbreviated as C4-xBxA3$ (x>0), presents even more satisfactory hydration properties than stoichiometric one. However, the hydration mechanism is not well understood, in particular for the effect of Ba/Ca ratio on hydration behavior. To shed light on this issue, high purity C4-xBxA3$ samples with designed element compositions (C4A3$, C3.5B0.5A3$, and C3BA3$) were prepared and their hydration processes were investigated. The results reveal that Ba-doped ye'elimite reacts faster than the stoichiometric ye'elimite. With the increase of Ba/Ca ratio, it can gradually increase the intensity of the initial peak, shorten the dormant period and reduce the total hydration heat. The phase composition evolution based on Rietveld/XRD method demonstrates that the dissolution rate of the C3.5B0.5A3$ and C3BA3$ are about 19% and 28% higher than that of C4A3$ in 6h. Moreover, the hydration sequences and main products varied significantly. The AFt is absent for the system with barium incorporation and AFm tends to be less with the increase of Ba/Ca ratio. This paper also proposes a new acceleration mechanism of Ba-doped ye'elimite. It is summarized as a higher rate of dissolution-precipitation reaction stemmed from higher ion precipitation of BaSO4 and a combination of extra surface for the nucleation sites provided by BaSO4.

Hydration mechanisms of Ba-doped ye'elimite: Effect of Ba/Ca ratio on hydration behavior

Piqi Zhao[1,*], Xingyuan Bao[1], Heng Chen[1], Shoude Wang[1,*], Lingchao Lu[2], A.G. De La Torre[3] and XinCheng [1,2]

[1] Shandong Provincial Key Laboratory of Preparation and Measurement of Building Materials, University of Jinan, Jinan 250022, China;

[2] School of Materials Science and Engineering, University of Jinan, Jinan 250022, China;

[3] Departamento de QuímicaInorgánica, Cristalografía y Mineralogía, Universidad de Málaga, Málaga 29071, Spain

* Correspondence: mse_zhaopq@ujn.edu.cn, mse_wangsd@ujn.edu.cn; Tel.: +86-531-8276-7217

ABSTRACT

Ba-doped ye'elimite, abbreviated as $C_{4-x}B_xA_3\$$ (x>0), presents even more satisfactory hydration properties than stoichiometric one. However, the hydration mechanism is not well understood, in particular for the effect of Ba/Ca ratio on hydration behavior. To shed light on this issue, high purity $C_{4-x}B_xA_3\$$ samples with designed element compositions ($C_4A_3\$$, $C_{3.5}B_{0.5}A_3\$$, and $C_3BA_3\$$) were prepared and their hydration processes were investigated. The results reveal that Ba-doped ye'elimite reacts faster than the stoichiometric ye'elimite. With the increase of Ba/Ca ratio, it can gradually increase the intensity of the initial peak, shorten the dormant period and reduce the total hydration heat. The phase composition evolution based on Rietveld/XRD method demonstrates that the dissolution rate of the $C_{3.5}B_{0.5}A_3\$$ and $C_3BA_3\$$ are about 19% and 28% higher than that of $C_4A_3\$$ in 6h. Moreover, the hydration sequences and main products varied significantly. The AFt is absent for the system with barium incorporation and AFm tends to be less with

the increase of Ba/Ca ratio. This paper also proposes a new acceleration mechanism of Ba-doped ye'elimite. It is summarized as a higher rate of dissolution-precipitation reaction stemmed from higher ion precipitation of $BaSO_4$ and a combination of extra surface for the nucleation sites provided by $BaSO_4$.

Keywords： ye'elimite; hydration mechanism; Rietveld; $C_{4-x}B_xA_3\$$

1. Introduction

Compare with PC, calcium sulphoaluminate (CSA) cement has such advantages as higher early strength, faster hardening and better anti-corrosion [1-3]. In addition, as it has a lower calcining temperature, it is proposed as environmentally friendly materials[4]. So far CSA has been well applied to many special engineering constructions. The reason for the superior performance of CSA is mainly due to the sulphoaluminate mineral ($4CaO·3Al_2O_3·SO_3$, abbreviated as $C_4A_3\$$ and also named ye'elimite)[5, 6]. More precisely, the high reactivity with water of this phase is attributed to the special crystalline structure with narrow gaps[7-9]. However, the properties of CSA still need to be further improved to meet the increasingly stringent requirements of modern applications. Some researchers proposed to introduce C_3S into the CSA system to improve early strength and cohesiveness[10, 11]. But this object is difficult to achieve due to the low decomposition temperature of $C_4A_3\$$ and the high formation temperature of C_3S, which leads to quite a narrow sintering range of coexistence. Prior studies demonstrated that doping with Ba^{2+} was a reasonable strategy to overcome this problem [12-14]. On the one hand, the doping with Ba^{2+} can not only reduce the time and temperature of C_3S formation but also improve the hydration reactivity of C_3S and C_2S[15, 16]. On the other hand, it can lead to the formation of new mineral of $C_{4-x}B_xA_3\$$ ($4\text{-}xCaO·xBaO·3Al_2O_3·SO_3$) with characteristics of

much higher early strength and better stability of hardening paste volume. More particularly, some researchers reported that the $C_{4-x}B_xA_3\$$ had a higher decomposition temperature than $C_4A_3\$$[17]. Hence, research on $C_{4-x}B_xA_3\$$ is important from the perspectives of basic and applied research. Chang [18, 19] demonstrated that Ba^{2+}led to irregular coordination in the crystalline structure of $C_4A_3\$$, resulting in volume distortion and improved hydration reactivity. Yan and Cheng[13, 20] reported that barium-containing ettringite was found in the hydration products of $C_{4-x}B_xA_3\$$. The quantum chemical analysis showed the bond level of Ba-O bond was higher than Ca-O, which made the bond strength of barium-containing ettringite higher than common ettringite, and the strength was enhanced.

Although ye'elimite modified by barium doping can significantly improve its hydration properties, the hydration and hardening process, especially the hydration mechanism, has not been elucidated. In keeping with this question, relative work is reviewed. The crystalline structure analysis of ye'elimite[21-24] has furnished persuade evidence that the high-temperature phase, which follows body-centered cubic symmetry, can be preserved at ambient temperatures by ions incorporation. Furthermore, they suggested that the incorporation of ion into the crystal lattice of ye'elimite had a significant effect on hydration behavior. Cuesta et al.[25] and Jansen et al. [26] reported that the hydration kinetics of ye'elimite depends on polymorphism of ye'elimite and Fe-doped solid solutions of ye'elimite hydrate faster than stoichiometric ones. Benarchid et al.[27] concluded that the chromium or phosphorous bearing $C_4A_3\$$ also has a significant effect on the stabilization of cubic type ye'elimite. However, the duration of the dormant period was significantly extended. One more important question to be answered from the present paper

emerges from the fact that the hydration behavior of ye'elimite would show a large variation with different types, bearing contents and impurity phases, even if they contain the same crystalline form [28-30]. About Ba-doped ye'elimite, very recent research has reported that the hydration process and products varied significantly with the stoichiometric one[28]. However, a detailed explanation of the different barium bearing contents that cause the hydration behavior is not yet available in the literature. Understanding the Ba-doped ye'elimite hydration mechanisms and differences in the hydration behavior affected by Ba/Ca ratio is the main motivation for this work. For this purpose, high purity $C_{4-x}B_xA_3\$$ (x=0, 0.5, 1) with designed element composition are prepared. A comparison of hydration behavior, including dissolution-precipitation reactions and hydration products evolution, is investigated. We also proposed a hydration mechanism based on the barium incorporation effect. This study is a step forward to better understanding the hydration behavior of Ba-doped ye'elimite systems.

2. Materials and methods

2.1 Raw materials

The analytical pure reagents of $CaCO_3$, $BaCO_3$, Al_2O_3 and $CaSO_4{\cdot}2H_2O$ (purity of 99.9%, fromSinopharm Chemical Reagent Co., Ltd, China) were used in this work to synthesize $C_{4-x}B_xA_3\$$. They were ground and sieved through 74μm before being used. Powder of corundum (α-Al_2O_3-SRM-676a, from National Institute of Standards and Technology(NIST), USA) was used as the internal standard to obtain phase composition of $C_{4-x}B_xA_3\$$ paste. Demineralized water was used in all hydration experiments.

2.2 Sample preparation

Mixtures of a stoichiometric proportion of the above chemical reagents were prepared to synthesize $C_{4-x}B_xA_3\$$, where x was set as 0, 0.5 and 1, respectively. The resulting powders were firstly ground in a planetary mill with absolute ethyl alcohol at 200r.p.m for 30min, then dried at 50℃, pelletized and finally calcined. The calcination system of target minerals($C_4A_3\$$, $C_{3.5}B_{0.5}A_3\$$, and $C_3BA_3\$$) were slightly varied and detailed in Table 1. Since the radius of Ba^{2+} (135pm) is much larger than that of Ca^{2+} (100pm), it requires much more energy to form Ba-doped ye'elimite. Therefore, in comparison with $C_4A_3\$$, we slightly increased the calcination temperature, heating preservation time and calcination time for $C_{3.5}B_{0.5}A_3\$$ and $C_3BA_3\$$, respectively, to guarantee the purities higher than 95wt%. The Rietveld refinement patterns and quantitative results were shown in Fig. 1 and Table 2. Only orthorhombic or cubic ye'elimite was detected in $C_4A_3\$$ and $C_3BA_3\$$, respectively, but there existed both orthorhombic and cubic ye'elimite in $C_{3.5}B_{0.5}A_3\$$. The minerals were ground in a planetary micro mill at 700 rpm for 3~5min. The specific surface area value (SSA_{BET}) of $C_4A_3\$$, $C_{3.5}B_{0.5}A_3\$$, and $C_3BA_3\$$ were detected as 0.47, 0.69 and 0.40 m^2/g, respectively. The EDS analysis of $C_{3.5}B_{0.5}A_3\$$ and $C_3BA_3\$$, shown in Fig. 2 with ten random points, demonstrated that the elemental composition of the target minerals basically meets the design expectations.

Table 1 Calcination system settings

Minerals	Calcination temperature/ ℃	Heating preservation time/ h	Cooling mode	Calcination times§
$C_4A_3\$$	1300	4	Air-cooling†	1
$C_{3.5}B_{0.5}A_3\$$	1350	6	Air-cooling	2
$C_3BA_3\$$	1380	6	Air-cooling	3

†Air-cooling means the samples were quenched in air from high temperatures.
§Calcination times mean the repetition number under the fixed calcination temperature and heating preservation time.

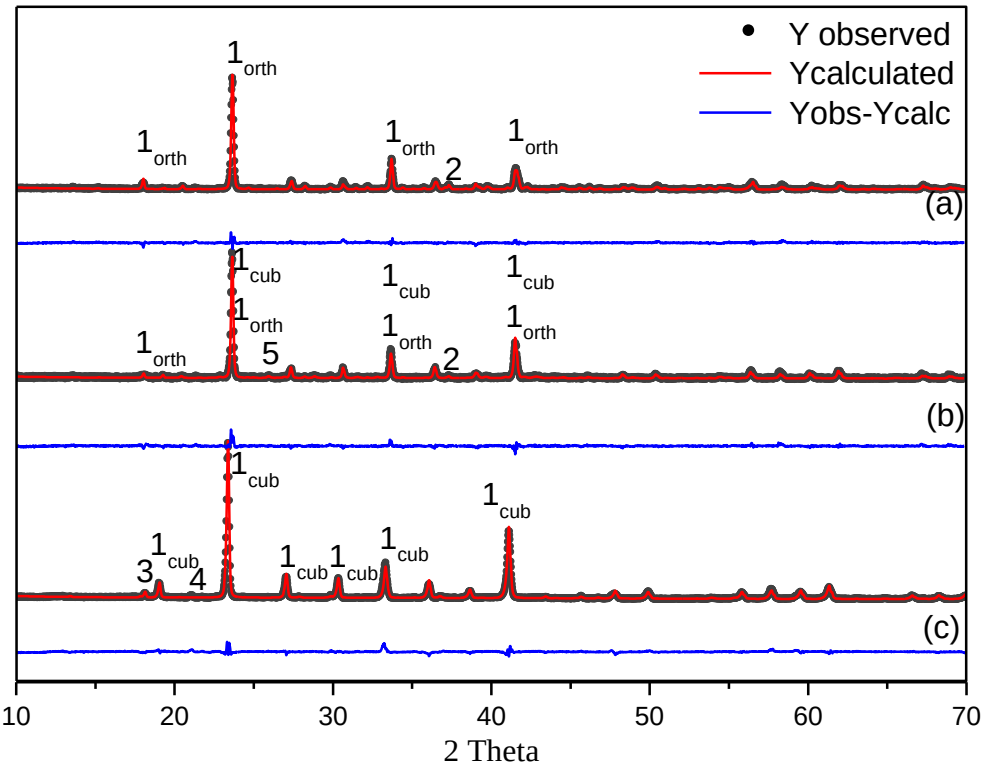

1_{orth}-ye'elimite_orthorhombic; **1_{cub}**-ye'elimite_cubic; **2**-f-CaO; **3**-$C_{12}A_7$; **4**-$BaAl_2O4$; **5**-$BaSO_4$

Fig .1 Rietveld refinement patterns of C_4A_3(a), $C_{3.5}B_{0.5}A_3$(b) and C_3BA_3(c)

Table 2 Rietveld quantitative phase analysis of C_4A_3(a), $C_{3.5}B_{0.5}A_3$(b) and C_3BA_3(c)

Analysis	**Phases and R-factors**	**C_4A_3**	**$C_{3.5}B_{0.5}A_3$**	**C_3BA_3**	**ICSD codes**
Quantitative results /Wt%	ye'elimite_orthorhombic	97.7(4)	44.9(5)	—	80361
	ye'elimite_cubic	—	52.2(5)	97.6(8)	81654
	f-CaO	2.3(2)	0.5(1)	—	60704
	$C_{12}A_7$	—	—	1.1(1)	29212
	$BaAl_2O_4$	—	—	1.3(1)	10036
	$BaSO_4$	—	2.4(2)	—	16904
Unite cell volume/ cm^3	ye'elimite_orthorhombic	3.87×10^{-22}	3.90×10^{-22}	—	—
	ye'elimite_cubic	—	3.92×10^{-22}	4.03×10^{-22}	—
Criteria of fit	R_{WP}[%]	12.41	13.98	10.64	—

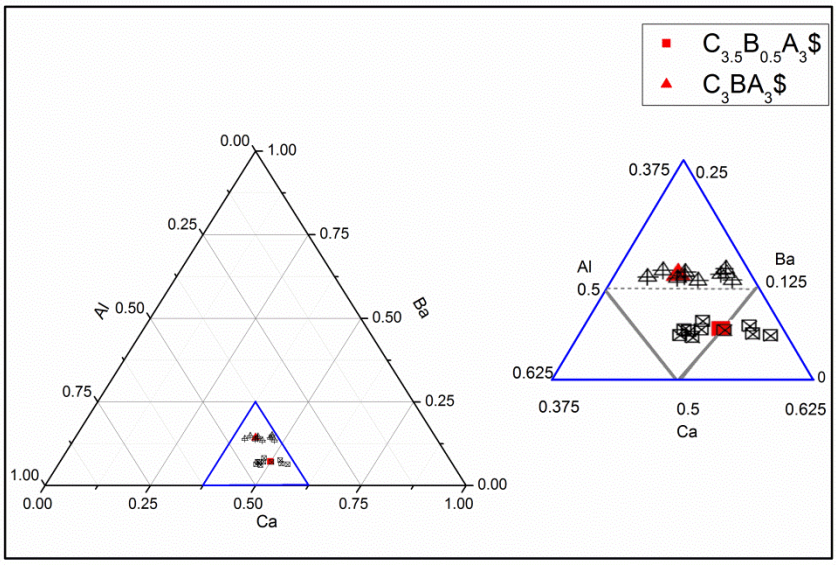

Fig .2 Electron probe microanalysis of $C_{4-x}B_xA_3$ composition. (The square and triangle represented the designed (in red) and calculated (in black) composition of C_3BA_3 and $C_{3.5}B_{0.5}A_3$, respectively.)

Hydrated pastes were prepared by using a deionized water-to-$C_{4-x}B_xA_3$ (w/c) ratio of 1.0. For each group, the paste was distributed to 5 polythene bottles, sealed and cured at 20 ± 1°C with rotation for uniformity of water distribution until curing ages (6, 12, 18, 24 and 48hours) were reached. Then they were quickly ground with enough ethyl alcohol, filtered with suction, alcohol washed and carefully dried at 40℃ in a vacuum drying cabinet until a constant weight is reached. Finally, these samples were stored in a closed desiccator to avoid further hydration or carbonation. For Rietveld quantitative analysis of hydrated samples (without free water), they were well mixed with α-Al_2O_3 as the internal standard. For quantitative analysis of free water in hydrated samples (without free water), the corresponding powers of the above curing ages were accurately weighed about 2 g (balance to the nearest 0.001 g) and placed in a ceramic crucible that has been calcined to constant weight. Then they were heated from room temperature to 900℃ with a rate of 10°/min.

After being kept at 900℃ for 1h, they are cooled to below 200℃ in the furnace and finally cooled to room temperature in a desiccator.

2.3 Experimental test

The X-ray powder diffraction (XRD) patterns were recorded in Bragg-Brentano reflection geometry (θ/2θ) on D8 ADVANCE (Bruker AXS) diffractometer. The detailed instrument settings for XRD are summarized in Table 3. The qualitative and quantitative phase assemblages of the anhydrous and hydrated samples were examined using Rietveld refinement analysis by TOPAS 4.2 software.

The hydration heat flow was measured with a conduction calorimeter (Thermometric TAM Air) at 25℃. Three measurements of 2 g of minerals ($C_4A_3\$$, $C_{3.5}B_{0.5}A_3\$$ and $C_3BA_3\$$) were carried out with a water/solid ratio of 1.0. After the reference samples were injected into the admix ampoule and equilibration was obtained, the demineralized water was injected into the reaction vessel and the samples were stirred in the calorimeter. It is noting that this procedure allowed monitoring the heat evolution from the very beginning. And the hydration heat flow was recorded for 24 h.

A conductimeter (MASHENGMP) was used to do conductivity measurements. The experiments were performed in diluted suspension, thermostated at 25℃ and continuously subjected to magnetic stirring. The water to solid ratio was equal to 10.

SEM images with EDS analysis were performed to observe the morphology of phases and elements distribution both in anhydrous samples and their hydration pastes. Wherein, the microstructure of hardened pastes cured for 24h was directly observed based on the bulk sample without any stopping hydration treatments. The version of the equipment was FEI QUANTA 450 and Oxford Link ISIS-300.

The initial pore water composition was measured quantitatively using ICP-MS(NexION 350X). The pastes were prepared by mixing 10g of $C_{4-x}B_xA_3\$$ and 10g of deionized water. The pore solution was obtained by centrifugation at 4000 rpm for 2 min and then filtered through a 200 nm filter. In all the cases, the filtration of the pore solution started after 5 min. Finally, it was acidified with HNO_3 to a certain ratio.

The density of target minerals was measured by the pycnometer method, thermostated at 25℃. A detailed description of the method can be found in[31, 32]. The specific surface area value was determined by an automated nitrogen gas sorption unit (Gemini VII 2390, Micromeritics) and the data were analyzed using the multipoint BET method[33].

Table3 XRD instrument settings

Parameter	Step scanning
X-ray radiation power	40 kV/40 mA
Wavelength type: $CuK\alpha_1$	$K\alpha_1$= 1.540598Å
Monochromator	Ge (111)
Detector	X´Celerator detector
Divergence slit (°)	1.00
Soller slit (rad)	0.04
Receiving slit (°)	0.6
Step width (°)	0.02
Measure time (h)	0.5
Scan range (2θ /°)	5-70

3. Results and discussion

3.1 Hydration heat evolution of $C_{4-x}B_xA_3\$$

The influence of Ba/Ca ratio on hydration heat flow of $C_{4-x}B_xA_3\$$ is shown in Fig. 3. Similar features can be characterized by other curves[34, 35], which are composed of two

exothermic peaks. The first occurs directly when the water is added and can be attributed to the solution heat and the early hydration reactions. The second one, followed by the induction period, covers the main part of the hydration reaction. The exact exothermic time and hydration heating value are shown in Table 4. With the increase of Ba/Ca ratio, the time of the initial reaction is basically the same. However, the hydration heating value increases significantly from 8.9J·g-1 to 20.2 J·g-1, indicating a stronger dissolution-precipitation reaction when Ca^{2+} is partially substituted by Ba^{2+}. Compare with the Period Ⅱ, the stoichiometric ye'elimite (C_4A_3\$), similar to the length of induction period in elsewhere[25], is prolonged by about 3.1h and 6.8h based upon $C_{3.5}B_{0.5}A_3$\$ and C_3BA_3\$ sample, respectively. It means the hydration is accelerated with the increase of Ba/Ca ratio. The hydration heat is mainly released in the acceleration period(Period Ⅲ), which decreases dramatically with the increase of Ba^{2+} dosage. And the total hydration heat of C_4A_3\$, $C_{3.5}B_{0.5}A_3$\$ and C_3BA_3\$ within 24h are 490.3J·g^{-1}, 370.8 J·g^{-1},and 251.5 J·g^{-1}, respectively. The hydration heat of C_3BA_3\$ is almost one half of the stoichiometric ye'elimite. Therefore, the effect of Ba/Ca ratio in $C_{4-x}B_xA_3$\$ on the hydration heat flow can be summarized as increasing intensity of the initial peak, shortening the induction period and significantly reducing the heat released in deceleration period.

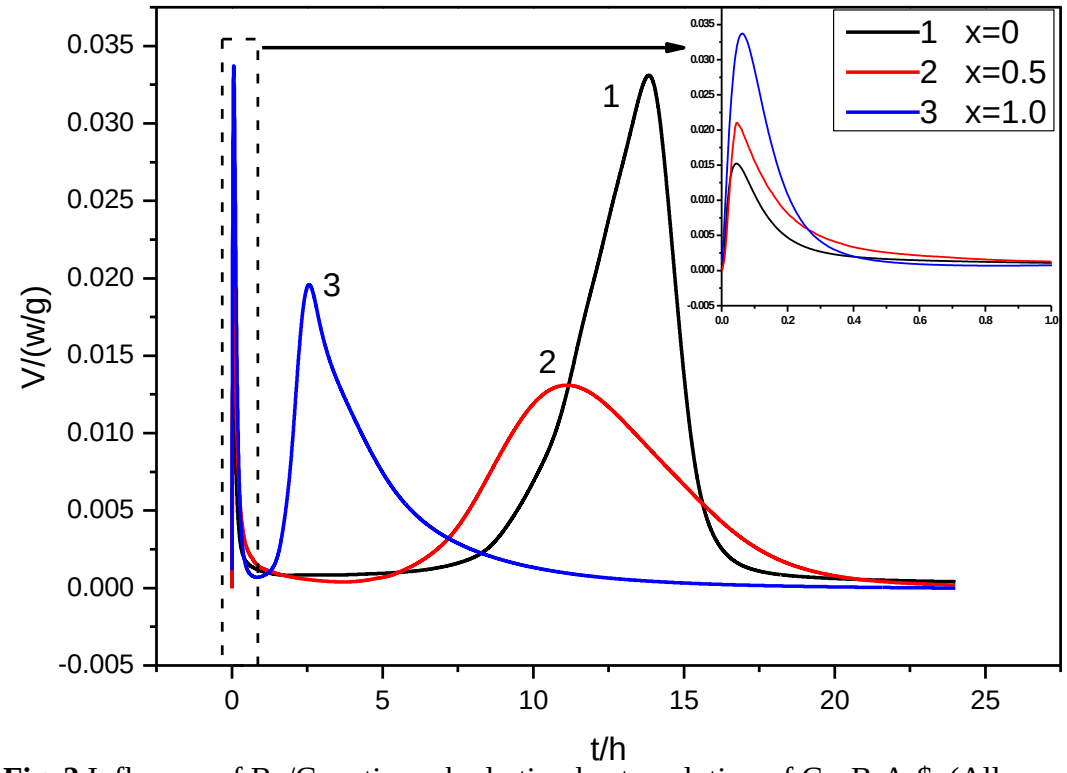

Fig .3 Influence of Ba/Ca ratio on hydration heat evolution of $C_{4-x}B_xA_3\$$. (All measurements were performed at 20℃ and the w/s ratios were kept at 1.0)

Table 4 $C_{4-x}B_xA_3\$$ exothermic time and hydration heating value

$C_{4-x}B_xA_3\$$	†Period Ⅰ		†Period Ⅱ		†Period Ⅲ		†Period Ⅳ(-24h)		Total heat / $J\cdot g^{-1}$
	time /h	heat/ $J\cdot g^{-1}$	time /h	heat/ $J\cdot g^{-1}$	time /h	heat/ $J\cdot g^{-1}$	time /h	heat/ $J\cdot g^{-1}$	
X=0	0.4	8.9	7.6	19.5	5.8	291.4	---	160.5	490.3
X=0.5	0.5	14.3	4.5	12.0	6.0	134.9	---	209.6	370.8
X=1	0.5	20.2	0.8	2.4	1.3	44.2	---	184.7	251.5

†Period Ⅰ, Ⅱ, Ⅲ and Ⅳ represent the initial reaction period, induction period, acceleration period and deceleration period, respectively.

3.2Electrical conductivity of $C_{4-x}B_xA_3\$$ suspension

Conductimetry is a powerful tool to monitor the hydration behavior[32, 36, 37]. The results of the electrical conductivity of $C_{4-x}B_xA_3\$$ suspension are plotted in Fig.4. Similar to

other cementitious minerals such as C_3S[38, 39], one obvious peak appears at early hydration time. The conductivity increases sharply at the beginning due to rapid ions release under the reactions between $C_{4-x}B_xA_3\$$ and water (Eq. 1). With the increase of Ba/Ca ratio, the peak values conductivity decrease, which indicates the solution concentrations of Ba-doped ye'elimite are less than the stoichiometric one in the initial dissolution period. It can be easily explained by the fact that some hydration products quickly reach saturation and precipitate out at the beginning of hydration. The prior study [29] has already demonstrated that AFt is a comparatively fast-precipitation hydration product in the ye'elimite hydration system. However, when the solution contains Ba^{2+}, it tends to form $BaSO_4$ rather than AFt to precipitate the SO_4^{2-}[40]. It means $BaSO_4$ will precipitate faster, which would be one explanation for the faster hydration rate of Ba-doped samples. Interestingly, the slopes of the conductivity curve at this stage are almost kept at a constant value, indicating that the substitution of Ba^{2+} in $C_4A_3\$$ has not significantly improved the dissolution rate at early hydration time, Eq.1. Subsequently, the conductivity drops due to the faster precipitation than dissolution. We notice that conductivity curves of $C_{3.5}B_{0.5}A_3\$$ and $C_3BA_3\$$ show a slightly different decrease trend as a function of Ba/Ca ratio. The negative slope value increases with the increment of Ba/Ca (inset of Fig. 4). This may indicate that the substitution of Ba^{2+} could promote the ion precipitation rate, Eq.2.

$$C_{4-x}B_xA_3\$+H_2O \rightarrow Ca^{2+}+Ba^{2+}+Al^{3+}+SO_4^{2-} \quad (1)$$

$$Ba^{2+}+SO_4^{2-} \rightarrow BaSO_4 \quad (2)$$

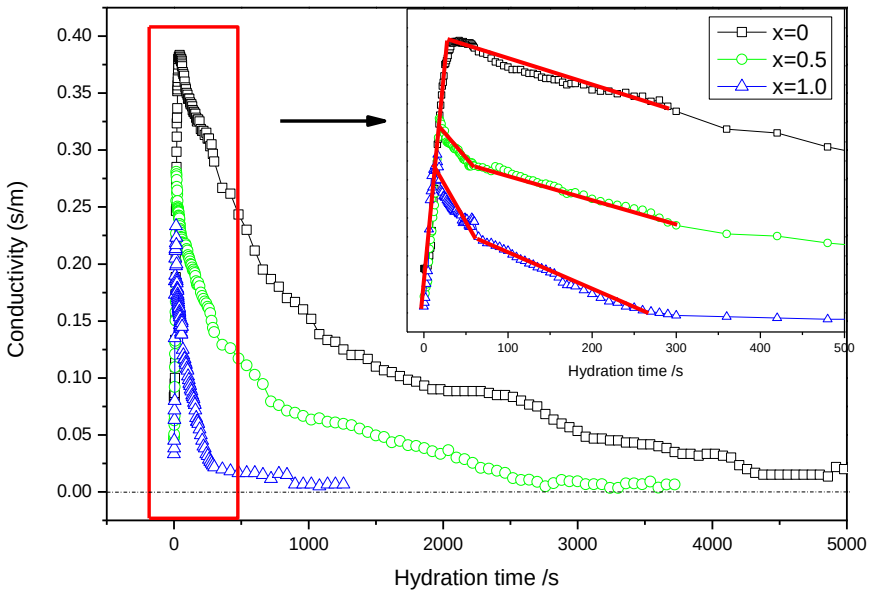

Fig .4 Influence of Ba/Ca ratio on the electrical conductivity of $C_{4-x}B_xA_3\$$. (All measurements were performed at 20℃ and the w/s ratio was kept at 10.0)

3.3 Quantitative characterization of hardened $C_{4-x}B_xA_3\$$ paste

To further understand the hydration mechanism, the phase composition evolution of hardened $C_{4-x}B_xA_3\$$ pastes was studied by Rietveld quantitative analysis with internal standard methodology. Before that, hydrated sample XRD patterns were firstly analyzed, identifying that both $BaSO_4$ and hydrated calcium aluminate (C_2AH_8 and CAH_{10}) were detected only in the sample of $C_{3.5}B_{0.5}A_3\$$ and $C_3BA_3\$$. On the contrary, AFt only existed in $C_4A_3\$$ paste. The other phases such as AFm and unhydrated ye'elimite appeared in all $C_{4-x}B_xA_3\$$ samples, but AFm tends to be less with the increase of Ba/Ca ratio. The main hydration products vary significantly with different Ba/Ca ratios. The reason can be inferred that barium incorporation alters the evolution of solution composition and hence affect the crystallization sequences of the hydration product. As discussed in the previous section, it is mainly because in combination with SO_4^{2-}, the hydration product $BaSO_4$ is

more likely to precipitate out than AFt and AFm. The selected XRD patterns ($C_{4-x}B_xA_3$_24h) are shown in Fig. 5. Afterward, the α-Al_2O_3 as the internal standard was well mixed with the hydrated sample, and the ratio of α-Al_2O_3 to the hydrated sample was fixed at 1:4. The XRD patterns were then recorded again and refined to obtain the quantitative results, Table 5. The selected refinement patterns of $C_{3.5}B_{0.5}A_3$_24h was shown in Fig. 6. Subsequently, amorphous and non-quantified crystalline phases (abbr. ACn, i.e., AH_3) was derived from the comparison between the actual dosage and Rietveld result of the internal standard, seen in Eq. 3[41]. Finally, the mass fraction of different components in $C_{4-x}B_xA_3$\$ paste was calculated based on the results above and free water analysis that was obtained from the chemical bonding water measurement. In addition, the free water was deduced based on Eq. 4-5 and the results of $C_{4-x}B_xA_3$_24h samples were selected and shown in Table 6.

$$\mathrm{ACn} = \frac{1\text{-}W_{st} / R_{st}}{100 - W_{st}} \times 10^4 \tag{3}$$

$$W_{CW} = \frac{m_1 - m_2}{m_1} \times 100\% \tag{4}$$

$$W_{FW} = 1 - \frac{1}{1 + w/c} \times \frac{1}{1 - W_{CW}} \tag{5}$$

Where W_{st} and R_{st} stand for the actual dosage and Rietveld results of the internal standard, respectively. W_{FW} and W_{CW} represent free water content in $C_{4-x}B_xA_3$\$ paste and chemical water content in the dried sample. m_1 and m_2 are the mass of hydration sample before and after combustion, respectively.

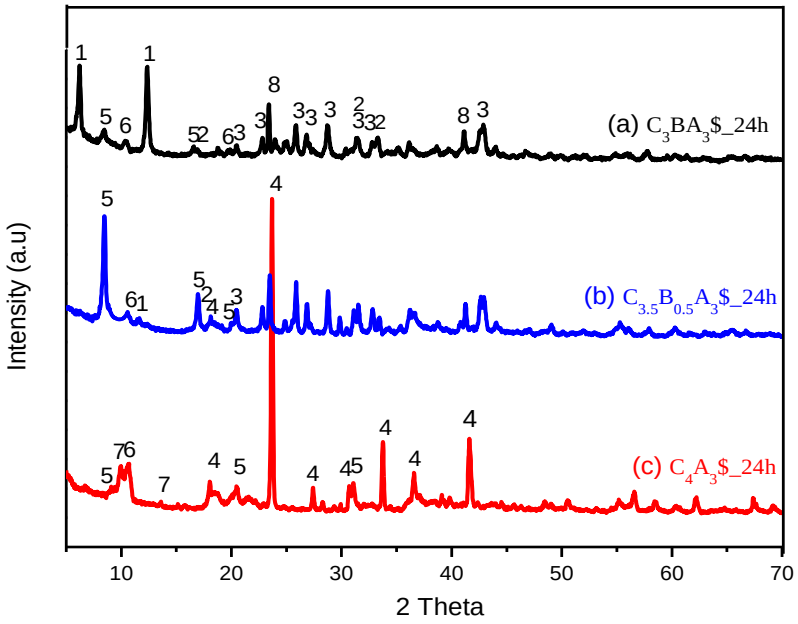

1-CAH_{10}, **2**-C_2AH_8, **3**-$BaSO_4$, **4**-ye'elimite_orthorhombic, **5**-AFm-c, **6**-AFm-n, **7**-AFt, **8**-ye'elimite_cubic

Fig .5 XRD patterns of hydrated $C_{4-x}B_xA_3\$$ samples at 24h (labeled as $C_4A_3\$$_24h (a), $C_{3.5}B_{0.5}A_3\$$_24h (b) and $C_3BA_3\$$_24h (c), respectively)

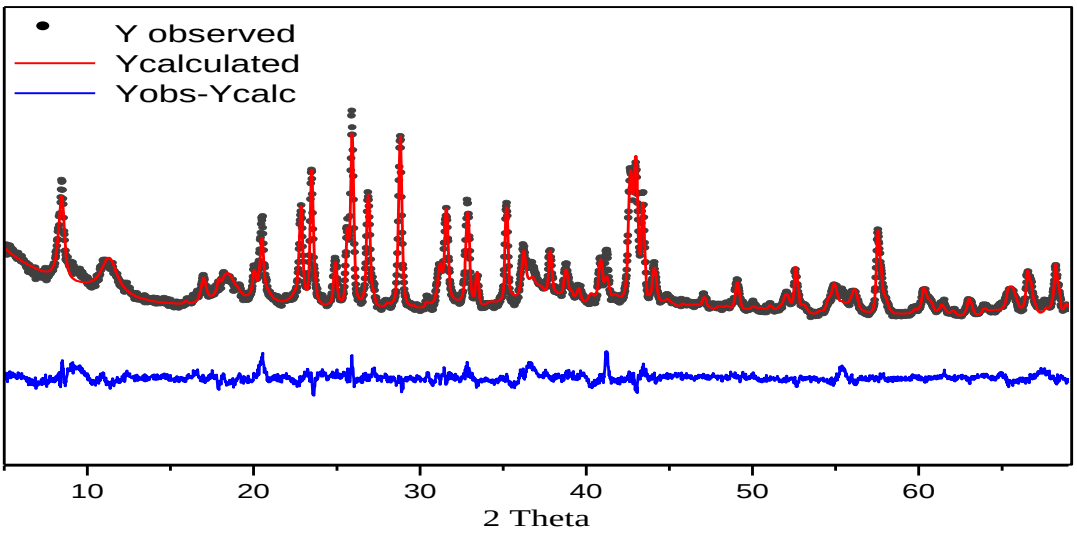

Fig .6 Rietveld refinement patterns of $C_{3.5}B_{0.5}A_3\$$_24h (b) with internal standard of α-Al_2O_3

Table 5 Rietveld quantitative results of $C_{4-x}B_xA_3\$$ samples at 24h

Analysis	Phases and R-factors	$C_4A_3\$$_24h	$C_{3.5}B_{0.5}A_3\$$_24h	$C_3BA_3\$$_24h	ICSD codes
Quantitative results /Wt%	ye'elimite_orthorhombic	13.7(5)	8.1(3)	none	80361
	ye'elimite_cubic	none	3.0(2)	7.9(2)	81654
	$BaSO_4$	none	10.1(2)	17.5(2)	16904
	AFm-c	11.1(4)	33.8(8)	8.2(3)	100138
	AFm-n	43.9(8)	18.2(6)	37.6(5)	100138
	AFt	6.4(3)	none	none	155395
	†C_2AH_8	none	present	present	none
	CAH_{10}	none	0.9(3)	3.9(2)	407150
	α-Al_2O_3	24.9(3)	25.8(4)	24.0(3)	73725
Criteria of fit	R_{wp}[%]	10.11	9.97	11.36	—
	R_{exp}[%]	4.34	4.87	4.98	—
	R_p[%]	7.76	6.87	7.10	—
	GOF	2.33	2.05	2.28	—

†Although C_2AH_8 was detected in Fig. 5, it was not included in this Rietveld quantitative analysis due to the lack of reported crystalline structure.

Table 6 Quantitative analysis of combined water and free water content

Sample	m_1/g	m_2/g	W_{CW} /%	W_{FW} /%
$C_4A_3\$$_24h	2.008	1.240	38.25	19.03
$C_{3.5}B_{0.5}A_3\$$_24h	2.056	1.182	42.51	13.03
$C_3BA_3\$$_24h	2.035	1.159	43.05	12.20

The quantitative phase composition of $C_{4-x}B_xA_3\$$ pastes, curing at 6, 12, 18, 24 and 48 hours were separately normalized, taking into account the free water deduced by the combined water measurement (Fig. 7). When Ba^{2+} is presented in ye'elimite, the formation of $BaSO_4$ as the essential hydration product leads to the reduction of SO_4^{2-} in the pore solution to be incorporated in further hydration products. This is the reason why the amounts of AFt and AFm decrease with the increase of Ba/Ca ratio and C-A-H, i.e. CAH_{10} and C_2AH_8 shows a tendency of increasing. The hydration degree of $C_{4-x}B_xA_3\$$, calculated with the Rietveld data normalized with free water, is depicted in Fig. 7(d). It can be inferred that the dissolution rate of $C_{4-x}B_xA_3\$$ is rapidly improved before 12 h and the trend

gradually slows down until it reaches the stable state after 18 h. Additionally, the increase of Ba/Ca ratio contributes to the improvement of the dissolution rate of ye'elimite, especially in the early hydration ages. $C_{3.5}B_{0.5}A_3\$$ and $C_3BA_3\$$ samples attain about 67 and 76% of hydration degree at 6 h, meanwhile, $C_4A_3\$$ is about 48% at that time. And there are no significant differences after 18 h. This effect has been corroborated by calorimetric measurements, see Fig. 4.

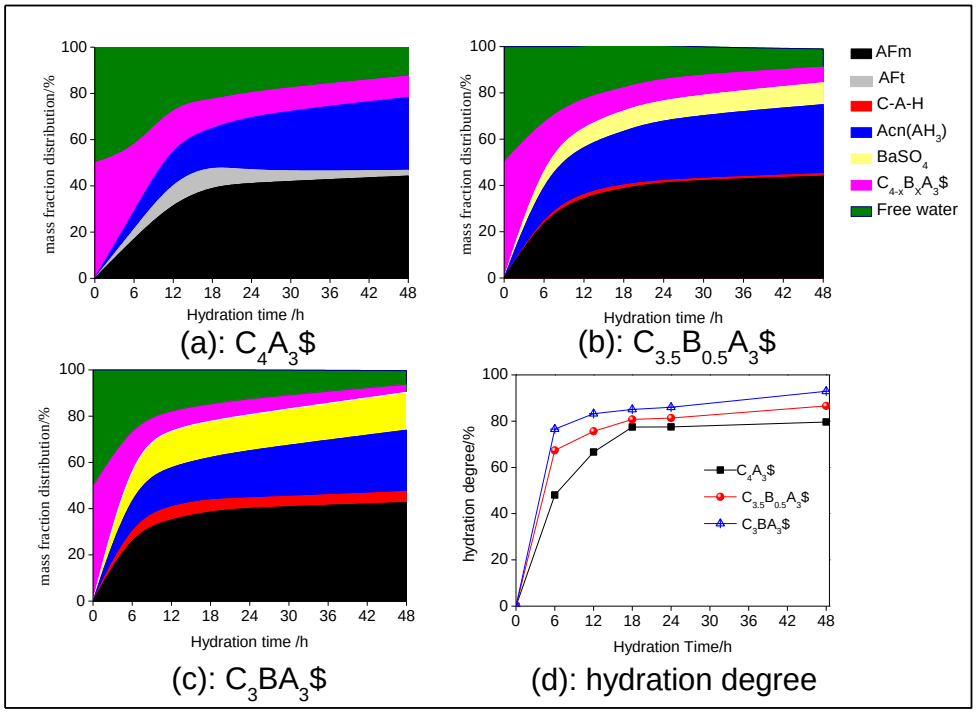

Fig .7 Quantitative phase analysis of hardened $C_{4-x}B_xA_3\$$ pastes and $C_{4-x}B_xA_3\$$ hydration degree.

3.4 SEM-EDS mapping analysis of hardened $C_{4-x}B_xA_3\$$ paste

The SEM images of $C_4A_3\$$_24h and $C_3BA_3\$$_24h samples are shown in Fig. 8(a) and (b), respectively. The AFm crystals with hexagonal-platelet morphology exist in both $C_4A_3\$$ and $C_3BA_3\$$ paste. Image J software was used to obtain the particle size from SEM images. It is observed that the particle size of AFm is similar in the above pastes, mostly

between 2μm and 5μm. However, partial AFt crystals with needle-like morphology are only present in $C_4A_3\$$ paste in aggregation state, which conforms with phase composition analysis above. The AH_3 phase in both $C_4A_3\$$ and $C_3BA_3\$$ paste show an agglomerated lamellar morphology. Similar results are also reported elsewhere[42], indicating that the AH_3 phase has a gibbsite-like morphology and also exhibits microcrystalline or nanocrystalline characteristics. It is also observed that the AH_3 phase randomly distributed among other phases with uniform particle size between 400nm and 800nm, seen in Fig. 8(b). It is possible to expect that an assembly of such interlocking clusters, obtaining good compatibility, would have potential good performance. However, AH_3 in $C_4A_3\$$ paste appears more prone to aggregation and the particle size is a little bit larger ranging from600 nm to 1500 nm. The selected SEM area of $C_3BA_3\$$ paste is shown in Fig.8(c) and elemental maps are depicted in Fig.8(d). It is observed that the Ca element is relatively uniform but distributed for less-density in four corners of this viewing zone. Combined with the other elemental maps, the corners circled in Fig. 8(d) (red square area labeled as ①~④, which is corresponding to area ①~④ in Fig .8(b)), showed relative Ba and S-rich area. The phase of $BaSO_4$ is inferred to be mainly present in these areas. Moreover, the morphological characteristics of the hydration products in Fig. 8b demonstrated that the selected area with red square is full of AH_3. It means there are some hydration products of $BaSO_4$ and AH_3 prone to form together.

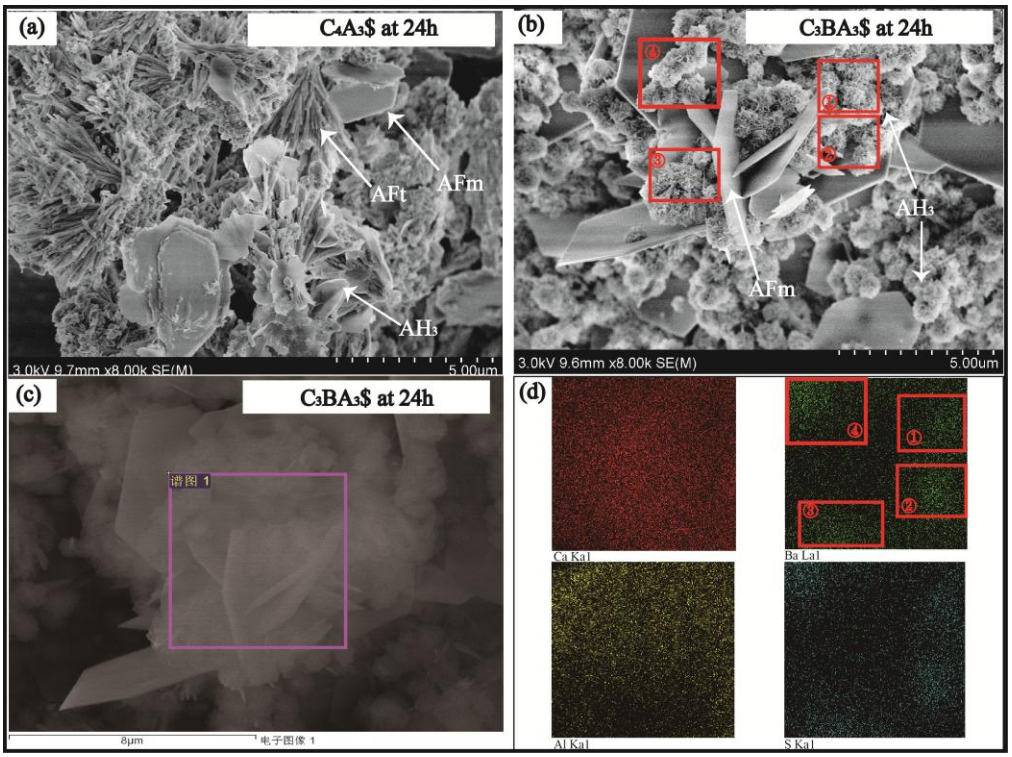

Fig .8 SEM images of C_4A_3\$_24h (a), C_3BA_3\$_24h (b) and the selected SEM area of C_3BA_3\$_24h (c) with EDS mapping (d)

3.5Proposed hydration mechanisms of $C_{4-x}B_xA_3$\$

Based on the analysis above, it can be stated that the early hydration of Ba-doped ye'elimite has significantly been accelerated. The leading cause at the first stage could be inferred as a higher ion precipitation rate. The precipitation mechanism related $BaSO_4$ could be active leading to a higher rate of heat evolution (seen in Table 4) and faster release of ions into solution (seen in Table 7, where it shows the concentration of Ca^{2+} in the system with Ba dosage is much higher than the reference sample of C_4A_3\$). Previous studies [43] demonstrated fast dissolution that happened in the initial period will lead to two-dimensional vacancy island, nucleation of small pits on the surface. And the dissolution rate in this stage is mainly related to the composition/structure of materials and

the solid-liquid interfacial energy[44]. Without considering the presence of defects or impurities, $C_{4-x}B_xA_3\$$ minerals would have a similar dissolution rate, which is also consistent with the electrical conductivity analysis above (Fig 5). The only difference between C_4A_3S and $C_{4-x}B_xA_3\$$ is that the hydration product $BaSO_4$ would quickly form on or near the surface of $C_{4-x}B_xA_3\$$, which in hence promotes the following clinker dissolution rate. Fig. 9 presents schematically the hydration process of $C_4A_3\$$ (a) and $C_{4-x}B_xA_3\$$ (b) at an early age of reaction.

Table 7 Ionic concentrations and pH value measured by means of ICP-MS and pH electrode in the system of $C_{4-x}B_xA_3\$$ hydration (hydration time=5min, Temperature=25℃, water to cement ration=1)

Analyte	Concentration		
	$C_4A_3\$$	$C_{3.5}B_{0.5}A_3\$$	$C_3BA_3\$$
Ca /mg·L^{-1}	883	1076	1139
Ba /mg·L^{-1}	---	779	823
Al /mg·L^{-1}	347	392	375
S /mg·L^{-1}	505	535	521
pH	10.7	10.9	10.9

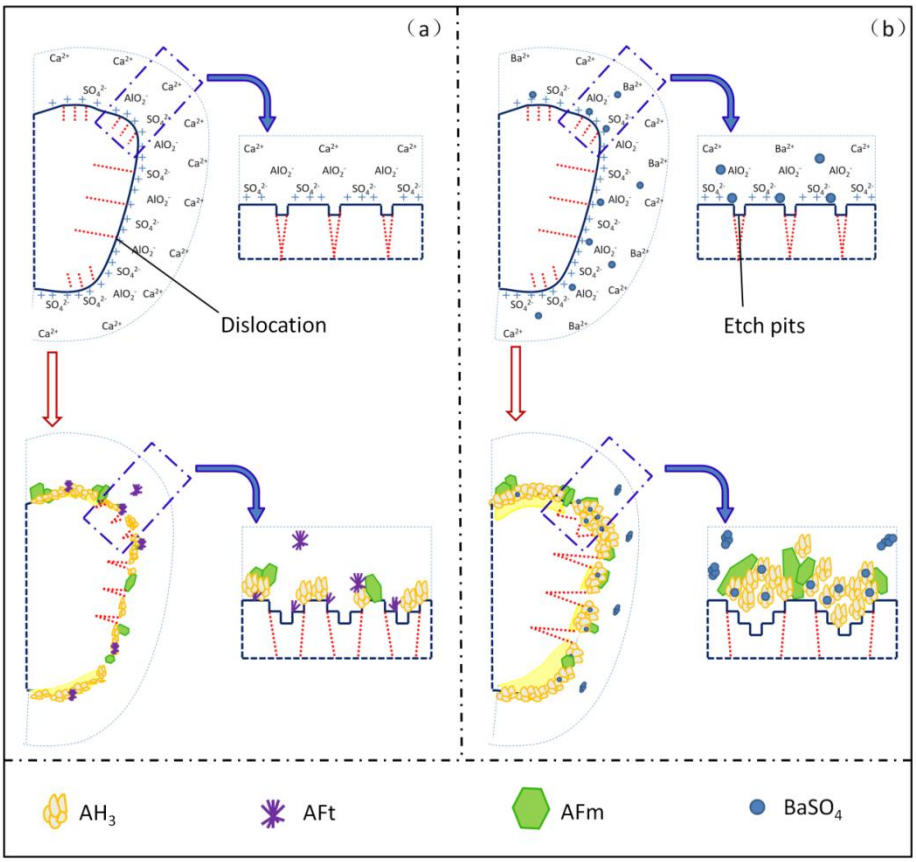

Fig.9 Hydration scheme of $C_4A_3\$$ (a) and $C_{4-x}B_xA_3\$$(b) at the early age of reaction.

After a few minutes, the ion concentration was significantly low despite the dissolution of the ye'elimite. The etch pits are present in abundance on the surface of minerals. As the large differences of hydration rate between $C_4A_3\$$ (a) and $C_{4-x}B_xA_3\$$, the etch pits of $C_{4-x}B_xA_3\$$ appear to be larger at the same hydration time. Finally, hydration products, such as AH_3, AFm and so on, start to grow. It is also interesting to note from EDS mapping analysis of $C_3BA_3\$\_24h$ (Fig. 8c,d) that some AH_3 gathered around $BaSO_4$. Another accelerating mechanism of $C_{4-x}B_xA_3\$$ is proposed that $BaSO_4$ might supply nucleation sites at the very early hydration time, as shown schematically in Fig. 9b. To further investigate it, a theoretical boundary nucleation and growth (BNG) model is used to analyze the calorimetric data (acceleration period and deceleration period) again. The

kinetic equation is as follows[45], which is widely used and well proved for C-S-H nucleation and growth[46-49].

$$X=1-\exp\left[-2O_V^B Gt+2O_V^B Gt\int_0^1 \exp\left(-\pi N_B G^2 t^2(1-m^2)\right)\mathrm{d}m\right] \quad (5)$$

Where X is the volume fraction of hydration products, O_V^B (in μm^{-1}) is the amount of substrate per unit volume, G (in $\mu m \cdot h^{-1}$) is the linear growth rate of hydration products, N_B (in μm^{-2}) is the amount of hydration product nuclei. Notably, O_V^B is not a fitting parameter, which can be calculated based on Eq. 6 and the results are shown in Table 5.

$$O_V^B = \frac{S}{{}^{w}/_{c}+{}^{1}/_{\rho}} \quad (6)$$

Where S is the specific surface area of the ground $C_{4-x}B_xA_3\$$ (BET method), ρ is the density, w/c is the water to minerals ratio.

Table 8 the calculated O_V^B values based on the specific surface area, density and water to minerals ratio of $C_{4-x}B_xA_3\$$

$C_{4-x}B_xA_3\$$	ρ/ $g \cdot cm^{-3}$	w/c	S/ m^2g^{-1}	O_v^B/ μm^{-1}
X=0	2.64	1.0	0.47	0.34
X=0.5	3.04	1.0	0.69	0.52
X=1	3.41	1.0	0.40	0.31

The fitting results are presented in Fig. 10. It can be seen that the Ba doping samples ($C_{3.5}B_{0.5}A_3\$$ and $C_3BA_3\$$) can be fitted very well with the BNG model, whereas that of the $C_4A_3\$$ shows unsatisfactory fitting. Table 6 presents the obtained fitting results of G and Ns of these heat curves. It can be seen that the number of nuclei (Ns) and linear growth rate of hydration products (G) increase with the substitution content of Ba^{2+} in $C_4A_3\$$, which further proves that the acceleration observed in the Ba doping system may stem from a

combination of extra surface for the nucleation provided by $BaSO_4$. However, the worse fitting result of $C_4A_3\$$ has not been resolved by now, and this might result from the difference in the growth mode of C-S-H and AFm and surface properties of C_3S and $C_4A_3\$$. This would be further investigated in our following research.

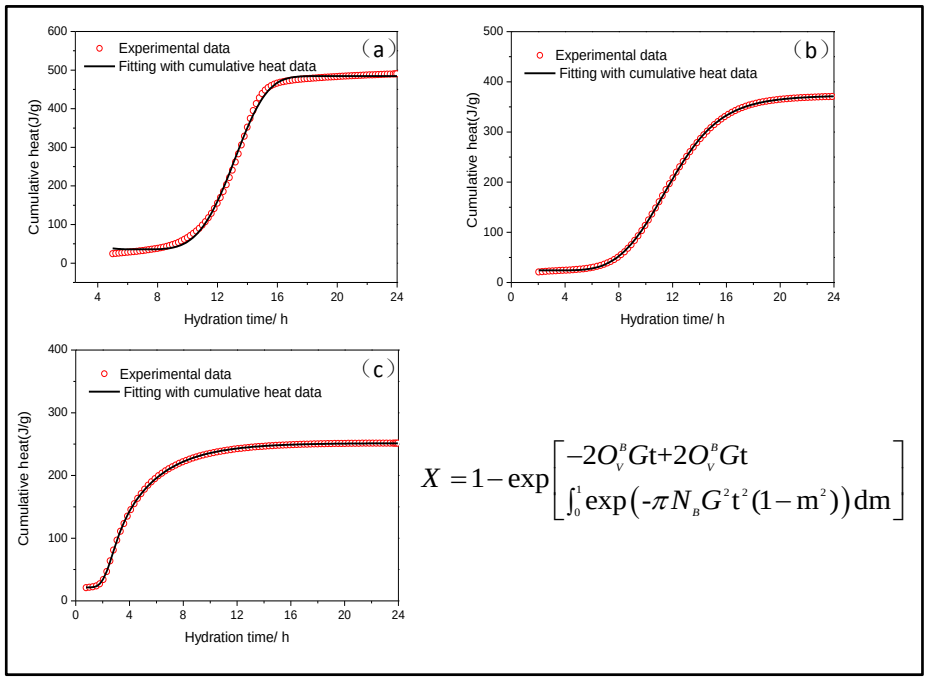

Fig.10 Results of data fitting by means of the kinetic model for $C_4A_3\$$ (a), $C_{3.5}B_{0.5}A_3\$$(b) and $C_3BA_3\$$ (c). The circles and solid lines represent the cumulative heat with respect to time, are the experimental data points and fitting curves obtained by Eq. 5, respectively.

Table 9 Linear growth rate, G, and the number of nuclei per unit surface, Ns, determined from the generalized BNG model fitting of hydration kinetics as a function of Ba^{2+} addition

$C_{4-x}B_xA_3\$$	G/ μm·h^{-1}	Ns/ μm^{-2}
X=0	Abnormal data	Abnormal data
X=0.5	0.24	1.60×10^{-1}
X=1	0.49	8.04×10^{-1}

4. Conclusions

First of all, it is worth highlighting that we have successfully synthesized the high purity $C_{4-x}B_xA_3\$$ with the designed element composition. And it is as expected that the barium incorporation has a significant effect on stabilization of cubic type ye'elimite and enlarging the cell volume. Moreover, this work reports some new data on the hydration mechanism and kinetics with respect to different Ba/Ca ratios in Ba-doped ye'elimite systems. Some detailed conclusions we would like to draw as follows,

(1)Ba-doped ye'elimite reacts faster than the stoichiometric ye'elimite. The lengths of the induction period of $C_{3.5}B_{0.5}A_3\$$ and $C_3BA_3\$$ are shortened by 3.1 and 6.8h compared with $C_4A_3\$$. The phase composition evolution based on Rietveld/XRD method also demonstrates that the dissolution rate of the $C_{3.5}B_{0.5}A_3\$$ and $C_3BA_3\$$ are about 19% and 28% higher than that of $C_4A_3\$$ in 6h.

(2) Ba-doped ye'elimite releases less heat than the stoichiometric ye'elimite. The total hydration heat of $C_3BA_3\$$ is only about one half of the stoichiometric ye'elimite.

(3) The hydration sequences and main products vary significantly with different Ba/Ca ratios. The AFt is absent for the system with barium incorporation in the selected curing ages and AFm tends to be less with the increase of Ba/Ca ratio. It is mainly because in combination with SO_4^{2-}, the hydration product $BaSO_4$ is more likely to precipitate out than AFt and AFm

(4) The accelerating mechanism of $C_{4-x}B_xA_3\$$ is proposed that firstly higher ion precipitation rate of $BaSO_4$ promotes the following dissolution-precipitation reaction. On the other hand, $BaSO_4$ might supply extra nucleation sites at the very early hydration time.

Acknowledgments

This work is supported by the National Natural Science Foundation of China (No.U1806222, 51602126, and 51761145023), National Key Research and Development Plan of China (No.2018YFD1101003 and No.2016YFB0303505), Key Laboratory of Advanced Civil Engineering Materials (Tongji University), Ministry of Education (202001), the Taishan Scholars Program, Case-by-Case Project for Top Outstanding Talents of Jinan, Youth Innovation Support Program of Shandong Colleges and Universities (2019KJA017), State Key Laboratory of Silicate Materials for Architectures (Wuhan University of Technology) (No.SYSJJ2018-12).

References

[1] X.J. Yang, J.S. Liu, H.X. Li, L.L. Xu, Q. Ren, L. Li, Effect of triethanolamine hydrochloride on the performance of cement paste, Constr Build Mater 200 (2019) 218-225.
[2] J. Péra, J. Ambroise, New applications of calcium sulfoaluminate cement, Cement and Concrete Research 34(4) (2004) 671-676.
[3] P. Zhang, F.H. Wittmann, M. Vogel, H.S. Muller, T.J. Zhao, Influence of freeze-thaw cycles on capillary absorption and chloride penetration into concrete, Cement and Concrete Research 100 (2017) 60-67.
[4] A.K. Chatterjee, High belite cements—Present status and future technological options: Part I, Cement and Concrete Research 26(8) (1996) 1213-1225.
[5] Hargis, W. Craig, Kirchheim, A. Paula, Monteiro, J.M. Paulo, M. Ellis, Early age hydration of calcium sulfoaluminate (synthetic ye'elimite, C4A3S) in the presence of gypsum and varying amounts of calcium hydroxide, Cement & Concrete Research 48 (2013) 105-115.
[6] A. Cuesta, G. Álvarez-Pinazo, S.G. Sanfélix, I. Peral, M.A.G. Aranda, A.G.D.L. Torre, Hydration mechanisms of two polymorphs of synthetic ye'elimite, Cement & Concrete Research 63 (2014) 127-136.
[7] A. Cuesta, A.G. De la Torre, E.R. Losilla, V.K. Peterson, P. Rejmak, A. Ayuela, C. Frontera, M.A.G. Aranda, Structure, Atomistic Simulations, and Phase Transition of Stoichiometric Yeelimite, Chemistry of Materials 25(9) (2013) 1680-1687.
[8] K. Ogawa, D.M. Roy, C 4 A 3 S hydration, ettringite formation, and its expansion mechanism: III. Effect of CaO, NaOH and NaCl; conclusions, Cement & Concrete Research 12(2) (1982) 247-256.
[9] M.J. Sanchez-Herrero, A. Fernandez-Jimenez, A. Palomo, C(4)A(3)S hydration in different alkaline media, Cement and Concrete Research 46 (2013) 41-49.
[10] X. Liu, Y. Li, N. Zhang, Influence of MgO on the formation of Ca3SiO5 and 3CaO·3Al2O3·CaSO4 minerals in alite–sulphoaluminate cement, Cement and Concrete Research 32(7) (2002) 1125-1129.
[11] S. Wang, C. Chen, L. Lu, X. Cheng, Effects of slag and limestone powder on the hydration and hardening process of alite-barium calcium sulphoaluminate cement, Construction and Building Materials 35 (2012) 227-231.
[12] C. Xin, Development and Application of Barium(Strontium) Calcium Sulphoaluminate Cement, J. Ceram. Soc. Chin (in Chinese) 30(1) (2015) 1458-1466.
[13] C. Xin, J. Chang, L.U. Lingchao, F. Liu, T. Bing, Study of Ba-bearing calcium sulphoaluminate minerals and cement, Cement & Concrete Research 30(1) (2000) 77-81.
[14] J. Chang, L. Lu, Y. Wang, C. Xin, Influence of Fluorite on Ba Bearing Sulphoaluminate Cement, Cement & Concrete Research 31(2) (2001) 213-216.
[15] N.K. Katyal, S.C. Ahluwalia, R. Parkash, Effect of barium on the formation of tricalcium silicate, Cement and Concrete Research 29(11) (1999) 1857-1862.

[16] X. Guo, L. Lu, S. Wang, Y. Chen, H. Wang, Influence of barium adding on composition and performance of alite-rich portland cement clinker, Journal of the Chinese Ceramic Society 37(12) (2009) 2083-2089.
[17] Y. Huang, S. Wang, P. Hou, Y. Chen, C. Gong, L. Lu, Mechanisms and kinetics of the decomposition of calcium barium sulfoaluminate, Journal of Thermal Analysis & Calorimetry 119(3) (2015) 1731-1737.
[18] J. Chang, study on ba-bearing calcium sulphoaluminate cement mineral, Journal of the Chinese Ceramic Society (1999).
[19] J. Chang, X. Shang, J. Zhao, Study on Sintering System of Calcium Barium Sulphoaluminate by XRD Quantitative Analysis, Applied Sciences-Basel 5(4) (2015) 989-997.
[20] P. Yan, Hydration of Sr-and Ba-bearing sulphoaluminates in the presence of sulphates, Advances in Cement Research 5(18) (1993) 65-69.
[21] O. Andac, F.P. Glasser, Polymorphism of calcium sulphoaluminate (Ca4Al6O16·SO3) and its solid solutions, Advances in Cement Research 6(22) (1994) 57-60.
[22] D. Kurokawa, S. Takeda, M. Colas, T. Asaka, P. Thomas, K. Fukuda, Phase transformation of Ca4[Al6O12]SO4 and its disordered crystal structure at 1073K, Journal of Solid State Chemistry 215 (2014) 265-270.
[23] S. Liu, X. Lu, J. Chen, S. Wang, Z. Ye, X. Cheng, Modulation of two ye'elimite phases via Ga3+ cation substitution, CrystEngComm 20(26) (2018) 3755-3764.
[24] A. Cuesta, Á.G. De la Torre, E.R. Losilla, I. Santacruz, M.A.G. Aranda, Pseudocubic Crystal Structure and Phase Transition in Doped Ye'elimite, Crystal Growth & Design 14(10) (2014) 5158-5163.
[25] A. Cuesta, G. Álvarez-Pinazo, S.G. Sanfélix, I. Peral, M.A.G. Aranda, A.G. De la Torre, Hydration mechanisms of two polymorphs of synthetic ye'elimite, Cement and Concrete Research 63 (2014) 127-136.
[26] D. Jansen, A. Spies, J. Neubauer, D. Ectors, F. Goetz-Neunhoeffer, Studies on the early hydration of two modifications of ye'elimite with gypsum, Cement and Concrete Research 91 (2017) 106-116.
[27] M.Y. Benarchid, J. Rogez, A. Diouri, A. Boukhari, J. Aride, Formation and hydraulic behavior of chromium–phosphorus doped calcium sulfoaluminate cement, Thermochimica Acta 433(1) (2005) 183-186.
[28] Y. Zhang, J. Chang, J. Zhao, Microstructural comparison of the AH 3 phase in the hydration of three structural modifications of ye'elimite, Journal of the American Ceramic Society 102(4) (2019) 2165-2175.
[29] F. Bullerjahn, M. Zajac, M. Ben Haha, K.L. Scrivener, Factors influencing the hydration kinetics of ye'elimite; effect of mayenite, Cement and Concrete Research 116 (2019) 113-119.
[30] M. Idrissi, A. Diouri, M.A. Talbi, O. Sassi, M. Taibi, D. Damidot, Hydration behavior of iron doped calcium sulfoaluminate phase at room temperature, MATEC Web of Conferences, EDP Sciences, 2012, p. 01005.
[31] V.K. Nagarajan, S.A. Devi, S. Manohari, M.M. Santha, Experimental study on partial replacement of cement with coconut shell ash in concrete, International Journal of science and research 3(3) (2014) 651-661.
[32] H. Li, H. Zhang, L. Li, Q. Ren, X. Yang, Z. Jiang, Z. Zhang, Utilization of low-quality desulfurized ash from semi-dry flue gas desulfurization by mixing with hemihydrate gypsum, Fuel 255 (2019) 115783.
[33] S. Brunauer, P.H. Emmett, E. Teller, Adsorption of Gases in Multimolecular Layers, Journal of the American Chemical Society 60(2) (1938) 309-319.
[34] F. Winnefeld, S. Barlag, Calorimetric and thermogravimetric study on the influence of calcium sulfate on the hydration of ye'elimite, Journal of Thermal Analysis & Calorimetry 101(3) (2010) 949-957.
[35] Y. Huang, C. Xu, H. Li, Z. Jiang, Z. Gong, X. Yang, Q. Chen, Utilization of the black tea powder as multifunctional admixture for the hemihydrate gypsum, Journal of Cleaner Production 210 (2019) 231-237.
[36] J. Pourchez, P. Grosseau, R. Guyonnet, B. Ruot, HEC influence on cement hydration measured by conductometry, Cement & Concrete Research 36(9) (2006) 1777-1780.
[37] J. Pourchez, P. Grosseau, B. Ruot, Current understanding of cellulose ethers impact on the hydration of CA and CA-sulphate systems, Cement & Concrete Research 39(8) (2009) 664-669.
[38] B. Bresson, F. Meducin, H. Zanni, C. Noik, Hydration of tricalcium silicate (C3S) at high temperature and high pressure.
[39] J. Pourchez, P. Grosseau, B. Ruot, Changes in CS hydration in the presence of cellulose ethers, Cement & Concrete Research 40(2) (2010) 179-188.
[40] P.M. Carmona-Quiroga, M.T. Blanco-Varela, Use of barium carbonate to inhibit sulfate attack in cements, Cement & Concrete Research 69 (2015) 96-104.

[41] A.G.D.L. Torre, S. Bruque, Aranda, Rietveld Quantitative Amorphous Content Analysis, Journal of Applied Crystallography 34(2) (2001) 196-202.
[42] F. Song, Z. Yu, F. Yang, Y. Lu, Y. Liu, Microstructure of amorphous aluminum hydroxide in belite-calcium sulfoaluminate cement, Cement and Concrete Research 71 (2015) 1-6.
[43] P. Juilland, E. Gallucci, R. Flatt, K. Scrivener, Dissolution theory applied to the induction period in alite hydration, Cement and Concrete Research 40(6) (2010) 831-844.
[44] P.M. Dove, N. Han, J.J. De Yoreo, Mechanisms of classical crystal growth theory explain quartz and silicate dissolution behavior, Proceedings of the National Academy of Sciences of the United States of America 102(43) (2005) 15357-62.
[45] G.W. Scherer, J. Zhang, J.J. Thomas, Nucleation and growth models for hydration of cement, Cement and Concrete Research 42(7) (2012) 982-993.
[46] S. Ghazizadeh, P. Duffour, N.T. Skipper, M. Billing, Y. Bai, An investigation into the colloidal stability of graphene oxide nano-layers in alite paste, Cement and Concrete Research 99 (2017) 116-128.
[47] G. Land, D. Stephan, The effect of synthesis conditions on the efficiency of C-S-H seeds to accelerate cement hydration, Cement and Concrete Composites 87 (2018) 73-78.
[48] J.J. Thomas, A New Approach to Modeling the Nucleation and Growth Kinetics of Tricalcium Silicate Hydration, Journal of the American Ceramic Society 90(10) (2007) 3282-3288.
[49] F. Ridi, E. Fratini, P. Luciani, F. Winnefeld, P. Baglioni, Tricalcium Silicate Hydration Reaction in the Presence of Comb-Shaped Superplasticizers: Boundary Nucleation and Growth Model Applied to Polymer-Modified Pastes, The Journal of Physical Chemistry C 116(20) (2012) 10887-10895.